Modeling and Measuring Dielectric Constants for Very Thin Materials Using a Coaxial Probe

K. Y. YOU[1], Z. ABBAS[2], C. Y. LEE[3], M. F. A. MALEK[4], K. Y. LEE[5], E. M. CHENG[6]

[1] Dept. of Radio Communication Engineering, Faculty of Electrical Engineering, Universiti Teknologi Malaysia, 81310 UTM Skudai, Malaysia
[2] Dept. of Physics, Faculty of Science, Universiti Putra Malaysia, 43400 UPM Serdang, Malaysia
[3]Faculty of Bioscience & Medical Engineering, Universiti Teknologi Malaysia
[4] School of Electrical Systems Engineering, Universiti Malaysia Perlis, Kuala Perlis, Perlis, Malaysia
[5]Dept. of Electrical and Electronic Engineering, Faculty of Engineering and Science, Universiti Tunku Abdul Rahman, 46200 Selangor, Malaysia
[6]School of Mechatronic Engineering, Universiti Malaysia Perlis, 02600 Arau, Perlis, Malaysia

kyyou@fke.utm.my, za@fsas.upm.edu.my, chiayew1@gmail.com, mfareq@unimap.edu.my, kylee@utar.edu.my, emcheng@unimap.edu.my

Abstract. *This paper is focused on the non-destructive measurement of the dielectric constants (relative permittivities) of thin dielectric material (0.1–0.5 mm) using an open-ended coaxial probe with an outer diameter of 4.1 mm. Normalized de-embedding and network error calibration procedures were applied to the coaxial probe. The measured reflection coefficients for the thin samples were taken with a vector network analyzer up to 7 GHz, and the calibrated reflection coefficients were converted to relative dielectric constants using an empirical reflection-coefficient model. The empirical model was created using the regression method and expressed as a polynomial model, and the coefficients of the model were obtained by fitting the data using the Finite Element Method (FEM).*

Keywords

Relative effective permittivity, one-port calibration, measured reflection coefficient, open-ended coaxial probe, thin dielectric substrate.

1. Introduction

Recently, there has been an increase of interest in the determination of the dielectric properties of thin samples in the microwave frequency range, such as conducting dielectric tests of thin-film materials in the fields of physics and engineering [1], as well as for the characterization of biological samples. In practice, the prime considerations in measuring the dielectric properties of the samples are the minimum thickness required to assume an infinite medium, the size of the sensor, limitations of the operational frequency, and the accuracy of the measurements.

Various two-port waveguide methods have been proposed for measuring the dielectric properties of thin materials, but some of those methods require specific dimensions for the thin-layer sample so that it will fit inside the given size of the waveguide [2], [3]. When using this method for thin samples, i.e., the thickness of the sample must be less than $\lambda/4$, it has been conventional practice to measure the reflection coefficient, Γ, and the transmission coefficient, T, by using the Nicholson-Ross-Weir (NRW) method [3], [4] or improved NRW routines [1], [5], [6]. Then, these measurements are converted to relative permittivity, ε_r, and relative permeability, μ_r, respectively. For non-destructive modification of the two-port measurement, for which the thin sample is placed between two aperture waveguides, the conversion process to acquire ε_r and μ_r requires a robust numerical analysis [7], [8].

Generally, an open-ended coaxial probe method is the simplest, broadband, non-destructive way to measure the dielectric properties of a material. This method is a one-port measurement that only measures the reflection coefficient, Γ, for the sample, and it is suitable for measuring the relative permittivity, ε_r, of the dielectric material (non-magnetic material, $\mu_r = 1$). However, a sample that has significant thickness is required for regular measurement in which an open-ended coaxial probe is used. This is required because the scattering of the wave from the probe's aperture would penetrate a very thin sample and impinge on the other layer-interface media. Normally, the sample is considered to be infinitely thick if its thickness, h, is as large as or larger than the diameter of the outer conductor, $2b$, for the coaxial probe (i.e., condition: $h \geq 2b$) [9]. Of course, a smaller and very slim coaxial probe could meet these needs for a thin-gauge material. But the uncertainty associated with fabricating a very small, slim, steel coaxial probe is significant, as is the uncertainty associated with the measurement of a thin sample (< 0.5 mm). In addition, the smallest commercial, coaxial waveguide available only has a $2b$ value of approximately 0.5 mm. Thus, this sensitive measurement could only be performed at very high

operational frequency (> 10 GHz) for a low-loss sample. In previous studies, the dielectric constant of a thin sample backed by metal plate was predicted from the measured reflection coefficient, Γ, via a quasi-static admittance model without involving the higher- order modes, TM_{0n} [10]. The reason is that an infinite higher-order series term of the quasi-static integration must be solved, which makes the calculations more complex. However, it is known that the higher order modes, TM_{0n}, occur due to the discontinuity-fringing effect at the aperture of the probe, which has a significant effect on the measured reflection coefficient, Γ, of very thin material (< 0.5 mm) backed by a metal plate.

In this paper, a model of an open-ended coaxial probe with three variables, i.e., sample thickness, h; relative dielectric constant, ε_r; and operational frequency, f, was formulated using the polynomial regression method. The parameters of the empirical model were estimated by fitting with simulated data obtained from COMSOL simulator, which implicitly takes into account the higher-order modes, TM_{0n}. The model can use measured reflection coefficients to predict the relative dielectric constant, ε_r, of samples that have thicknesses in the range of 0.1 to 0.5 mm. In this work, the diameter of the outer conductor, $2b$, of the study probe was 4.1 mm. A detailed description of the model and the measurement setup are provided in Sections 2 and 3, respectively.

2. Empirical Model Based on the Reflection Coefficient

In this work, the model of the complex reflection coefficient, Γ, of the coaxial probe sensor for obtaining measurements of thin samples was written in the form of a fifth-order polynomial:

$$\begin{aligned}\Gamma &= \Re\mathrm{e}(\Gamma) + j\Im\mathrm{m}(\Gamma) \\ &= \left(A_6 f^5 + A_5 f^4 + A_4 f^3 + A_3 f^2 + A_2 f + A_1\right) \\ &\quad + j\left(B_6 f^5 + B_5 f^4 + B_4 f^3 + B_3 f^2 + B_2 f + B_1\right)\end{aligned} \tag{1}$$

where f is the operational frequency (Hz). The polynomial coefficients (A_1, A_2, A_3, A_4, A_5, and A_6) for the real part of the reflection coefficient, Γ', are expressed in terms of the relative dielectric constant, ε_r, and the thickness of the sample, h (mm) as:

$$\begin{aligned}A_1 &= \varepsilon_r^4 \sum_{n=0}^{5} \eta_{24+n} h^n + \varepsilon_r^3 \sum_{n=0}^{5} \eta_{18+n} h^n + \varepsilon_r^2 \sum_{n=0}^{5} \eta_{12+n} h^n \\ &\quad + \varepsilon_r \sum_{n=0}^{5} \eta_{6+n} h^n + \sum_{n=0}^{5} \eta_n h^n\end{aligned}$$

$$\begin{aligned}A_2 &= \varepsilon_r^4 \sum_{n=0}^{5} \alpha_{24+n} h^n + \varepsilon_r^3 \sum_{n=0}^{5} \alpha_{18+n} h^n + \varepsilon_r^2 \sum_{n=0}^{5} \alpha_{12+n} h^n \\ &\quad + \varepsilon_r \sum_{n=0}^{5} \alpha_{6+n} h^n + \sum_{n=0}^{5} \alpha_n h^n\end{aligned}$$

$$\begin{aligned}A_3 &= \varepsilon_r^4 \sum_{n=0}^{5} \beta_{24+n} h^n + \varepsilon_r^3 \sum_{n=0}^{5} \beta_{18+n} h^n + \varepsilon_r^2 \sum_{n=0}^{5} \beta_{12+n} h^n \\ &\quad + \varepsilon_r \sum_{n=0}^{5} \beta_{6+n} h^n + \sum_{n=0}^{5} \beta_n h^n\end{aligned}$$

$$\begin{aligned}A_4 &= \varepsilon_r^4 \sum_{n=0}^{5} \gamma_{24+n} h^n + \varepsilon_r^3 \sum_{n=0}^{5} \gamma_{18+n} h^n + \varepsilon_r^2 \sum_{n=0}^{5} \gamma_{12+n} h^n \\ &\quad + \varepsilon_r \sum_{n=0}^{5} \gamma_{6+n} h^n + \sum_{n=0}^{5} \gamma_n h^n\end{aligned}$$

$$\begin{aligned}A_5 &= \varepsilon_r^4 \sum_{n=0}^{5} \sigma_{24+n} h^n + \varepsilon_r^3 \sum_{n=0}^{5} \sigma_{18+n} h^n + \varepsilon_r^2 \sum_{n=0}^{5} \sigma_{12+n} h^n \\ &\quad + \varepsilon_r \sum_{n=0}^{5} \sigma_{6+n} h^n + \sum_{n=0}^{5} \sigma_n h^n\end{aligned}$$

$$\begin{aligned}A_6 &= \varepsilon_r^4 \sum_{n=0}^{5} \chi_{24+n} h^n + \varepsilon_r^3 \sum_{n=0}^{5} \chi_{18+n} h^n + \varepsilon_r^2 \sum_{n=0}^{5} \chi_{12+n} h^n \\ &\quad + \varepsilon_r \sum_{n=0}^{5} \chi_{6+n} h^n + \sum_{n=0}^{5} \chi_n h^n\end{aligned} \tag{2a}$$

Similarly, the coefficients (B_1, B_2, B_3, B_4, and B_5) for the imaginary part of the reflection coefficient, Γ'', are written as:

$$\begin{aligned}B_1 &= \varepsilon_r^4 \sum_{n=0}^{5} \zeta_{24+n} h^n + \varepsilon_r^3 \sum_{n=0}^{5} \zeta_{18+n} h^n + \varepsilon_r^2 \sum_{n=0}^{5} \zeta_{12+n} h^n \\ &\quad + \varepsilon_r \sum_{n=0}^{5} \zeta_{6+n} h^n + \sum_{n=0}^{5} \zeta_n h^n\end{aligned}$$

$$\begin{aligned}B_2 &= \varepsilon_r^4 \sum_{n=0}^{5} \xi_{24+n} h^n + \varepsilon_r^3 \sum_{n=0}^{5} \xi_{18+n} h^n + \varepsilon_r^2 \sum_{n=0}^{5} \xi_{12+n} h^n \\ &\quad + \varepsilon_r \sum_{n=0}^{5} \xi_{6+n} h^n + \sum_{n=0}^{5} \xi_n h^n\end{aligned}$$

$$\begin{aligned}B_3 &= \varepsilon_r^4 \sum_{n=0}^{5} \psi_{24+n} h^n + \varepsilon_r^3 \sum_{n=0}^{5} \psi_{18+n} h^n + \varepsilon_r^2 \sum_{n=0}^{5} \psi_{12+n} h^n \\ &\quad + \varepsilon_r \sum_{n=0}^{5} \psi_{6+n} h^n + \sum_{n=0}^{5} \psi_n h^n\end{aligned}$$

$$B_4 = \varepsilon_r^4 \sum_{n=0}^{5} \tau_{24+n} h^n + \varepsilon_r^3 \sum_{n=0}^{5} \tau_{18+n} h^n + \varepsilon_r^2 \sum_{n=0}^{5} \tau_{12+n} h^n + \varepsilon_r \sum_{n=0}^{5} \tau_{6+n} h^n + \sum_{n=0}^{5} \tau_n h^n$$

$$B_5 = \varepsilon_r^4 \sum_{n=0}^{5} \upsilon_{24+n} h^n + \varepsilon_r^3 \sum_{n=0}^{5} \upsilon_{18+n} h^n + \varepsilon_r^2 \sum_{n=0}^{5} \upsilon_{12+n} h^n + \varepsilon_r \sum_{n=0}^{5} \upsilon_{6+n} h^n + \sum_{n=0}^{5} \upsilon_n h^n$$

$$B_6 = \varepsilon_r^4 \sum_{n=0}^{5} \rho_{24+n} h^n + \varepsilon_r^3 \sum_{n=0}^{5} \rho_{18+n} h^n + \varepsilon_r^2 \sum_{n=0}^{5} \rho_{12+n} h^n + \varepsilon_r \sum_{n=0}^{5} \rho_{6+n} h^n + \sum_{n=0}^{5} \rho_n h^n \quad (2b)$$

The values with twelve decimals for the complex coefficients of η_n, ζ_n (unity), α_n, ξ_n (in f^{-1}), β_n, ψ_n (in f^{-2}), γ_n, τ_n(in f^{-3}), σ_n, υ_n (in f^{-4}), and χ_n, ρ_n (in f^{-5}) are listed in Tab. 1 and Tab. 2 in the Appendix. The subscript n is the order of the coefficients. The complex values were obtained by fitting the coefficients with the calculated values of the reflection coefficients obtained from the finite-element method (FEM) using the commercial COMSOL simulator. The values of the coefficients were valid only for Teflon-filled coaxial probes with an inner conductor diameter, $2a$, of 1.3 mm and an outer conductor diameter, $2b$, of 4.1 mm, satisfying the relative dielectric constant, ε_r, from 1.8 to 20; the thickness of the sample, h, ranged from 0.1 to 0.5 mm; and the operational frequency ranged from 0.5 to 7 GHz. The fitting procedure of equation (1) can be described using five steps as follows:

Step 1:

The relationship between the real part of the reflection coefficient, Re(Γ), and operating frequency, f, is fitted using fifth-order polynomial regression, and the values of A_1, A_2, A_3, A_4, A_5, and A_6 were determined for a certain dielectric constant, ε_r, and sample thickness, h. The regression expression was:

$$\Re\mathrm{e}(\Gamma) = A_6 f^5 + A_5 f^4 + A_4 f^3 + A_3 f^2 + A_2 f + A_1 \ . \quad (3)$$

Step 2:

Step 1 was repeated to obtain the values of A_1, A_2, A_3, A_4, A_5, and A_6 for each dielectric constant ($\varepsilon_r = 1.5$, $\varepsilon_r = 2$, … , $\varepsilon_r = 15$) for a certain sample thickness, h.

Step 3:

All values of all of the coefficients (A_1, A_2, A_3, A_4, A_5, and A_6) obtained from Step 2 were fitted respectively with the corresponding dielectric constant, ε_r, using a fourth-order polynomial regression for a certain sample thickness, h. For instance, the regression analyses were expressed as:

$$\begin{aligned} A_1 &= a_4 \varepsilon_r^4 + a_3 \varepsilon_r^3 + a_2 \varepsilon_r^2 + a_1 \varepsilon_r + a_o \\ A_2 &= a_9 \varepsilon_r^4 + a_8 \varepsilon_r^3 + a_7 \varepsilon_r^2 + a_6 \varepsilon_r + a_5 \\ &\vdots \qquad\qquad \vdots \\ A_6 &= a_{29} \varepsilon_r^4 + a_{28} \varepsilon_r^3 + a_{27} \varepsilon_r^2 + a_{26} \varepsilon_r + a_{25} \end{aligned} \quad (4)$$

Step 4:

Step 3 was repeated to obtain the values of a_0, a_1, a_2,..., a_{28}, and a_{29} for each sample thickness (h = 0.1, 0.15, … , 0.5 mm).

Step 5:

Again, the relationship between each of the values of the coefficient (a_o, a_1, a_2, … , a_{29}) and the corresponding sample thickness, h, was determined using a fifth-order polynomial regression. For instance, the regression analyses were expressed as:

$$\begin{aligned} a_{\mathrm{o}} &= \eta_5 h^5 + \eta_4 h^4 + \eta_3 h^3 + \eta_2 h^2 + \eta_1 h + \eta_o \\ &= \sum_{n=0}^{5} \eta_n h^n \\ a_1 &= \eta_{11} h^5 + \eta_{10} h^4 + \eta_9 h^3 + \eta_8 h^2 + \eta_7 h + \eta_6 \\ &= \sum_{n=0}^{5} \eta_{6+n} h^n \\ &\vdots \qquad\qquad \vdots \\ a_{29} &= \chi_{29} h^5 + \chi_{28} h^4 + \chi_{27} h^3 + \chi_{26} h^2 + \chi_{25} h + \chi_{24} \\ &= \sum_{n=0}^{5} \chi_{24+n} h^n \end{aligned} \quad (5)$$

Substituting (5) into (4) yields (2a). The same procedures were used to determine the relationship between the imaginary part of reflection coefficient, Im(Γ), and the three parameters (f, ε_r, and h).

Fig. 1 shows the real part, Re(Γ), and the imaginary part, Im(Γ), of the reflection coefficients obtained from (1) and FEM simulation for various thicknesses, h, of the samples covering 0.5 to 7 GHz at room temperature. Overall, the samples were thinner and the Re(Γ) and Im(Γ) lines were more curved over the frequency range of 0.5 to 7 GHz. For a thin sample with a high dielectric constant (ε_r = 15), the Im(Γ) had a minimum value at a certain operational frequency at which the values changed from decreasing to increasing, as shown in Fig. 1. As a result, the average percentage of the relative error between the calculated and FEM-simulated values for both Re(Γ) and Im(Γ) was less than 2 % when the FEM simulation results were used as the reference value.

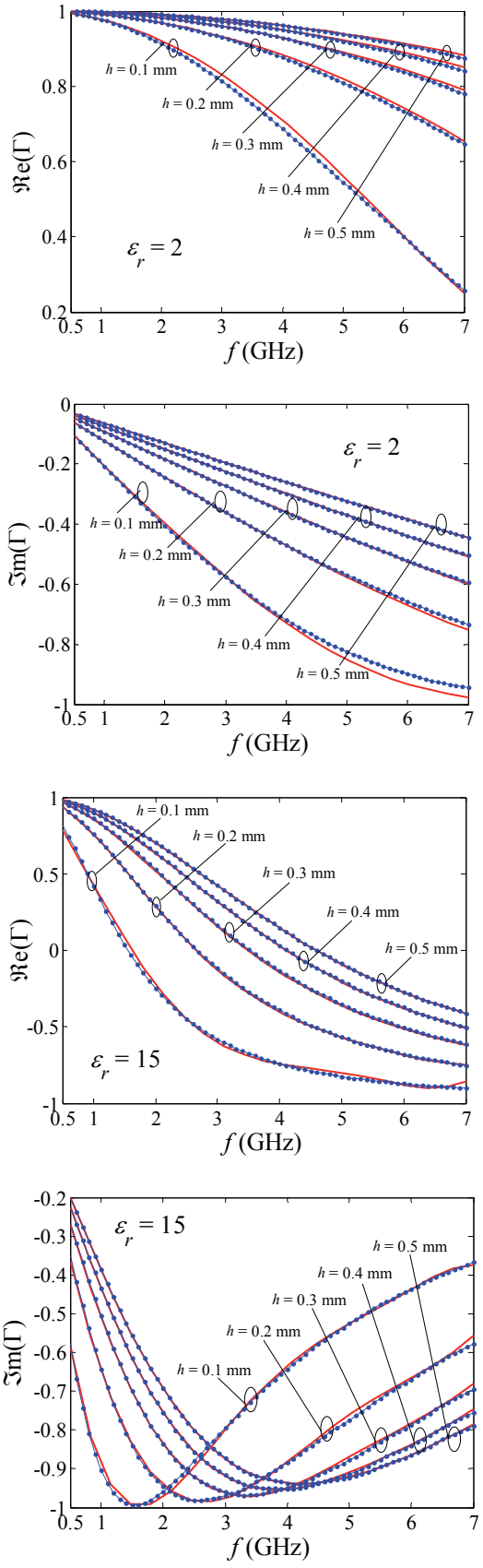

Fig. 1. Variations in Re(Γ) and Im(Γ) with frequency, f, for samples with various thicknesses, h: (Note: ---- Eq. (1); -•- FEM simulation).

3. Experimental Setup

The coaxial probe was fabricated from a 12.7 mm× 12.7 mm square flange; the SMA stub contact panel is shown in Fig. 2. The diameters of the inner and outer conductors were 1.3 and 4.1 mm, respectively, and the actual physical coaxial line was 7.6 mm. The coaxial line was filled with Teflon with a dielectric constant, ε_c, of 2.06. The measurements of the reflection coefficients, $\Gamma_{AA'}$, were made using a coaxial probe that consisted of an Agilent E5071C network analyzer in the frequency range of 0.5 to 7 GHz at room temperature, (25 ± 1)°C. In this study, a full, one-port calibration technique was implemented at the AA' plane using an Agilent 85052D 3.5-mm calibration kit (offset open, short, and load). Two techniques were used to calibrate the coaxial probe at the BB' aperture, i.e., 1) a normalized de-embedding technique using an air standard and 2) an errors-network model using three kinds of standard media [12], [13].

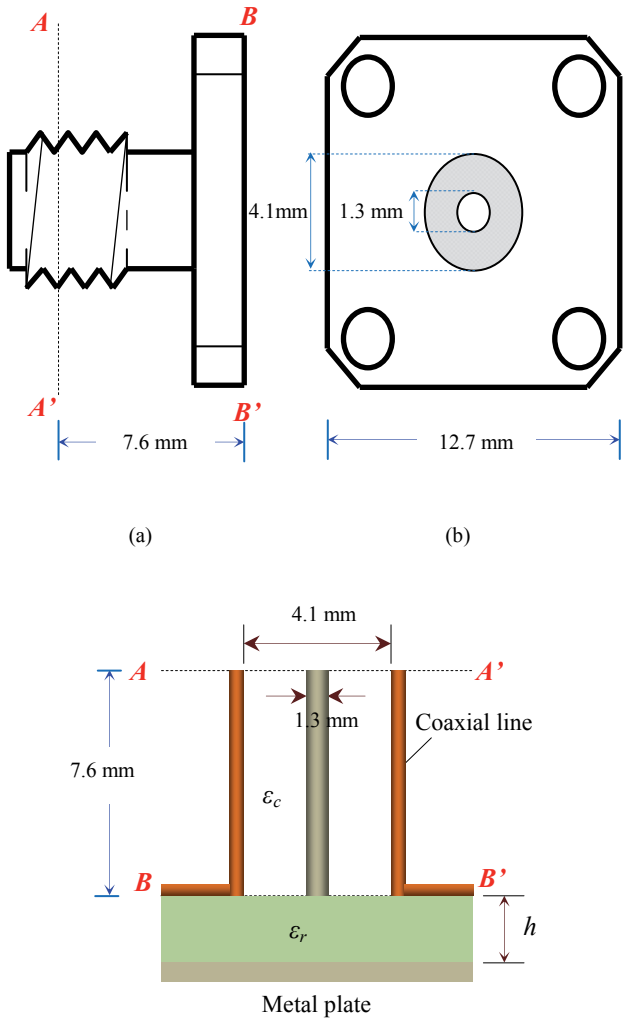

Fig. 2. Coaxial probe: (a) cross-sectional view; (b) front view; (c) experimental setup.

3.1 Normalized De-embedding Technique

In this work, a normalized de-embedding formulation (6) was used to calibrate the coaxial probe, and the formulation can be expressed as:

$$\Gamma_{BB'} = \Gamma_{AA'}\left(\frac{\Gamma_{Air\_FEM}}{\Gamma_{Air}}\right), \tag{6}$$

where Γ_{Air} is the reflection coefficient measurements for air at plane AA', and Γ_{Air_FEM} is the standard values of the air reflection coefficients at plane BB', obtained by using the finite element method (COMSOL simulator). Later, the reflection coefficient, $\Gamma_{BB'}$, was measured with the aperture of the probe placed against a two-layer medium, and the first layered medium to be tested was a thin sample with thickness, h, and the second layered medium was the conducting plate. As is well known, the standing wave error is not taken into account in normalized de-embedding calibration techniques. The standing wave that occurred in the coaxial line was caused mainly by fringing effects at the probe aperture, which was in direct contact with the sample. The standing wave effect can be ignored when the length of the operational quarter wave, $\lambda/4$, in the coaxial line is equal to or larger than the physical length, z, of the coaxial line. In this study, the error effect in the probe calibration can be neglected up to 7 GHz, the operational frequency at which $\lambda/4 = c/(4f\sqrt{\varepsilon_c}) \approx 7.6$ mm, which is equal to the physical length ($z = 7.6$ mm) of the probe being studied.

3.2 Network Error Techniques

The network error relationship between the measured reflection coefficient, $\Gamma_{BB'}$, and the actual reflection coefficient, $\Gamma_{AA'}$, for the sample being tested can be written as a bilinear equation [11], [12]:

$$\Gamma_{BB'} = \frac{\Gamma_{AA'} - C_2}{-C_3\Gamma_{AA'} + C_1} \tag{7}$$

where C_1, C_2, and C_3 are unknown complex calibration coefficients that were determined and optimized by using three calibration standards. In this study, air, liquid methanol, and pure water were used as the standards. Equation (7) can be rewritten as a linear expression:

$$C_1\Gamma_{BB'} + C_2 - \Gamma_{BB'}\Gamma_{AA'}C_3 = \Gamma_{AA'}. \tag{8}$$

Let $\Gamma_{BB'\_Air}$, $\Gamma_{BB'\_Methanol}$, and $\Gamma_{BB'\_Water}$ represent the known reflection coefficients for the air, methanol, and water standards, which terminate at the aperture plane BB', while, $\Gamma_{AA'\_Air}$, $\Gamma_{AA'\_Methanol}$, and $\Gamma_{AA'\_Water}$ are the measured reflection coefficients for air, methanol, and water at port AA'. Three sets of linear equations were developed and written in matrix form as:

$$\begin{bmatrix} \Gamma_{BB'\_Air} & 1 & -\Gamma_{BB'\_Air}\Gamma_{AA'\_Air} \\ \Gamma_{BB'\_Methanol} & 1 & -\Gamma_{BB'\_Methanol}\Gamma_{AA'\_Methanol} \\ \Gamma_{BB'\_Water} & 1 & -\Gamma_{BB'\_Water}\Gamma_{AA'\_Water} \end{bmatrix}\begin{bmatrix} C_1 \\ C_2 \\ C_3 \end{bmatrix} = \begin{bmatrix} \Gamma_{AA'\_Air} \\ \Gamma_{AA'\_Methanol} \\ \Gamma_{AA'\_Water} \end{bmatrix} \tag{9}$$

The values of $\Gamma_{BB'\_Air}$, $\Gamma_{BB'\_Methanol}$, and $\Gamma_{BB'\_Water}$ at the aperture (plane BB') for the air, methanol, and water were obtained from FEM simulation. In the simulation, the relative permittivity, ε_r, of air was unity. The relative permittivities, ε_r, of methanol and water were computed by the Cole-Cole model as:

$$\varepsilon_r = \varepsilon_\infty + \frac{\varepsilon_s - \varepsilon_\infty}{1 + (j\omega\tau)^{1-\alpha}}. \tag{10}$$

Methanol had parameters of $\varepsilon_s = 33.7$, $\varepsilon_\infty = 4.45$, $\tau = 4.95\cdot10^{-11}$ s, and $\alpha = 0.036$, and water had $\varepsilon_s = 78.6$, $\varepsilon_\infty = 4.22$, $\tau = 8.8\cdot10^{-12}$ s, and $\alpha = 0.013$ [13]. Equation (9) was solved by using a Gaussian elimination routine. Once the values of C_1, C_2, and C_3 were obtained, the calibrated reflection coefficient, $\Gamma_{BB'}$, of the thin sample backed by the conducting plate can be calculated by using (7). The accuracy of the network error calibration depended on the similarities between the values of ε_r obtained from (10) and the measured standard liquids. In this study, a short standard was not involved in the probe calibration. The reason was that the interference at the aperture of the probe was terminated by short circuits, which directly affected the measured $\Gamma_{BB'}$ due to the shorter length of study probe's coaxial line (plane AA' and BB' is closed). The above condition caused the open (air) and short standards to fail to maintain 180° of phase separation throughout the operational frequency range (especially at low operational frequencies).

4. Inverse Trial Function

In this work, after various functions were tried, two trial functions were recommended since both of the functions were able to provide more stable inverse results for all operating frequencies (0.5 to 7 GHz). Trial function (11a) represents the deviation of the ratio Re(Γ)/Im(Γ). Function (11b) is sum of the two deviation terms, i.e., the linear deviation term and the second term is the same as in function (11a). The predicted values of relative dielectric constant, ε_r', of the thin sample were obtained by minimizing the difference between the measured reflection coefficient, $\Gamma_{BB'}$, and the calculated Γ using (1) and by referring to the trial function, Λ:

$$\Lambda = \sum_{1}^{Data} \left\{ \frac{\Re\mathrm{e}(\Gamma)}{\Im\mathrm{m}(\Gamma)} - \frac{\Re\mathrm{e}(\Gamma_{BB'})}{\Im\mathrm{m}(\Gamma_{BB'})} \right\} \tag{11a}$$

or

$$\Lambda = \sum_{1}^{Data} \left\{ \begin{aligned} &\left[\Im\mathrm{m}(\Gamma) - \Im\mathrm{m}(\Gamma_{BB'}) \right] \\ &+ \left[\frac{\Re\mathrm{e}(\Gamma)}{\Im\mathrm{m}(\Gamma)} - \frac{\Re\mathrm{e}(\Gamma_{BB'})}{\Im\mathrm{m}(\Gamma_{BB'})} \right] \end{aligned} \right\} \tag{11b}$$

MATLAB's 'fzero' command was used to determine the zero routine. The initial approximate value in the numerical prediction was 5. The value of the relative dielectric constant, ε_r', of the thin sample was influenced by the real part of the reflection coefficient, Re(Γ), and, equally important, by the imaginary reflection coefficient, Im(Γ). For instance, the variations in the Re(Γ) and Im(Γ) of the probe with frequency, f, and relative dielectric constant, ε_r', for the sample with the thickness of 0.2 mm backed by a metallic plate are shown in Fig. 3.

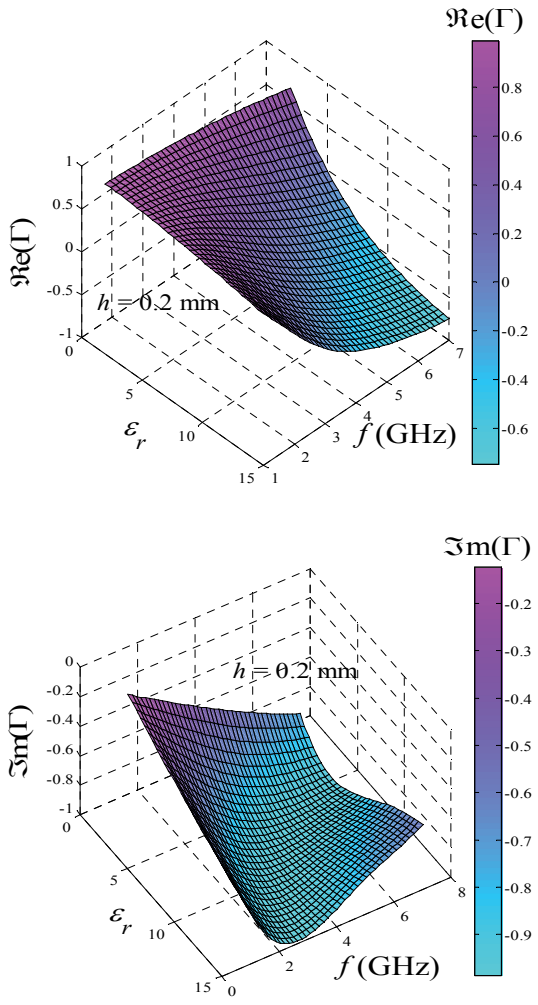

Fig. 3. Variation in Re(Γ) and Im(Γ) of water at 26°C with frequency f and inner radial of probe a.

5. Results and Discussion

To validate the results of the study, a thin layer of propan-1-ol liquid backed by metallic plate was measured using the experimental setup, as shown in Fig. 4.

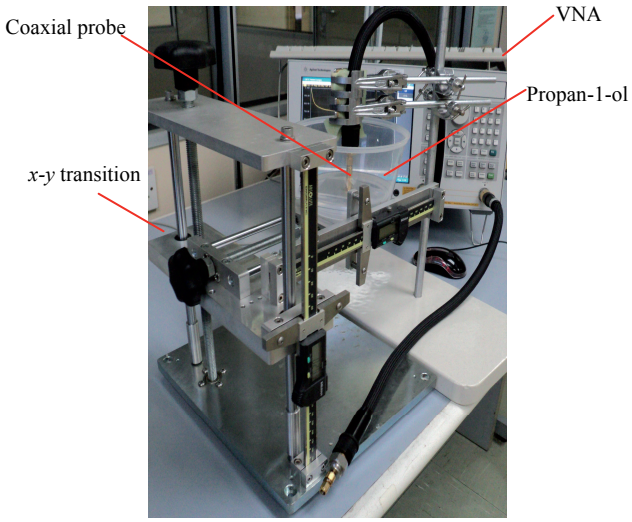

Fig. 4. Measurements of thin layer of propan-1-ol liquid aided by the x-y transition platform.

The reflection coefficient measurements (Re(Γ), Im(Γ), and Re(Γ)/Im(Γ)) of propan-1-ol liquid at 4 GHz were compared with the results obtained from finite element computation and (1) are shown in Fig. 5. The thickness of the propan-1-ol liquid layer was adjusted accurately based on the distance that the metallic plate moved away from the aperture of the probe in the propan-1-ol liquid using the x-y transition. The value of relative permittivity ($\varepsilon_r = 4.49 - j\,2.77$) of propan-1-ol in the simulation and in the calculation was obtained from infinite propan-1-ol liquid measurement using a Keysight (formerly Agilent) 85070D dielectric probe.

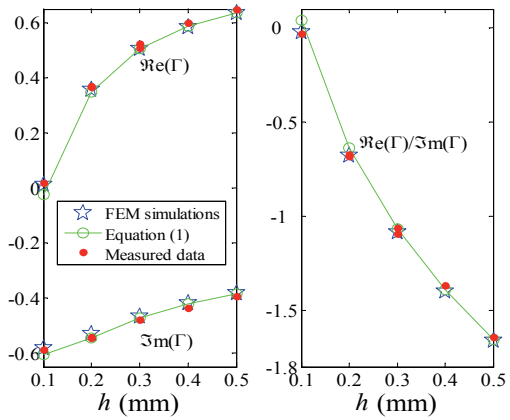

Fig. 5. Variation in Re(Γ), Im(Γ), and Re(Γ)/Im(Γ) of propan-1-ol liquid ($\varepsilon_r = 4.49 - j\,2.77$) with layer thickness h for 4 GHz at room temperature.

The absolute errors in the measured reflection coefficient were based on the difference between the measurements and the results calculated by (1), as shown in Fig. 6(a). The absolute error may have been caused by the sensitive measurements and high uncertainty in the controlled environment for the smaller-scale thickness of propan-1-ol liquid. The relative dielectric constant, ε_r', which was calculated from the measured reflection coefficient using (1) and trial function (11a), is shown in Fig. 6(b). The inverse values of ε_r' were found to be in relatively good agreement with the reference data, especially for $h \geq 0.2$ mm.

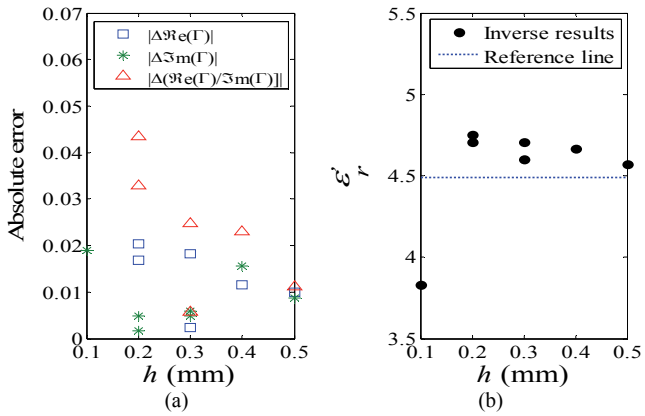

Fig. 6. (a) Variation in absolute measurement errors. (b) Corresponding inverse values of ε_r' for the thickness of the propan-1-ol liquid backed by metallic plate at 4 GHz.

Furthermore, we tested four unknown samples, i.e., *A* (h = 0.37 mm), *B* (h = 0.127 mm), *C* (h = 0.26 mm), and *D* (h = 0.27 mm). The measured Re(Γ) and Im(Γ) were compared with the calculated results, and the FEM simulation for validation is shown in Fig. 7. In the measurements, the four samples were considered to be homogeneous and isotropic. For the calculation and simulation of the Re(Γ) and Im(Γ) for samples *A*, *B*, *C*, and *D* in Fig. 7, it was assumed that the values of ε_r' were 2.2, 1.8, 4.8, and 8.5, respectively.

The difference between the calibrated reflection measurements by using normalized de-embedding and network error calibration techniques with the simulation results may have been caused by the properties of the materials that were obtained from the Cole-Cole model [13], since the assumptions made in the simulations may not exactly represent the actual properties of the materials. The variations in relative dielectric constant, ε_r', of the four samples with the operational frequency, f, are plotted in Fig. 8. The relative dielectric constants, ε_{r_meas}, were the inverse of the measured Re($\Gamma_{BB'}$) and Im($\Gamma_{BB'}$) and in referring to the trial function of (11b). Obviously, the predicted dielectric constants, ε_{r_meas} for samples *A*, *B*, *C*, and *D* , were in good agreement with the expected values (ε_r = 2.2, 1.8, 4.8, and 8.5).

Fig. 9 shows the values of ε_r' that were converted from the calibrated reflection coefficient (network error

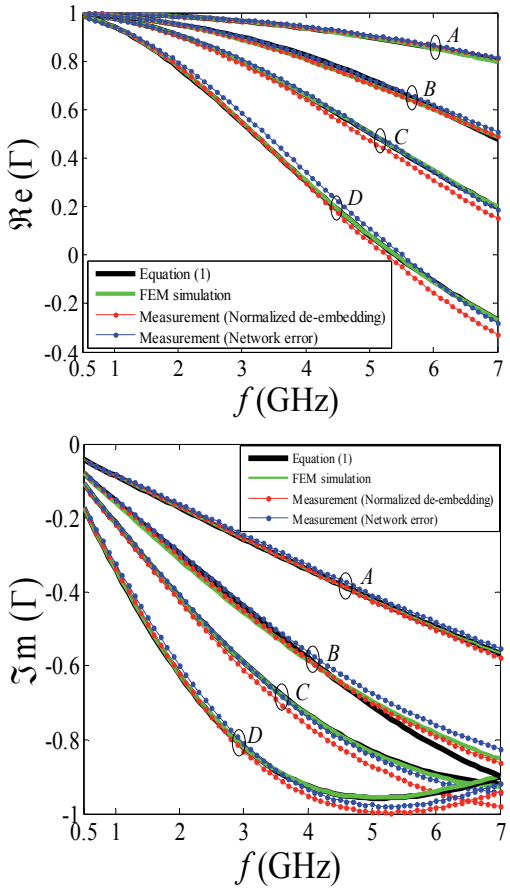

Fig. 7. Variations in Re(Γ) and Im(Γ) with frequency, f, for four unknown samples.

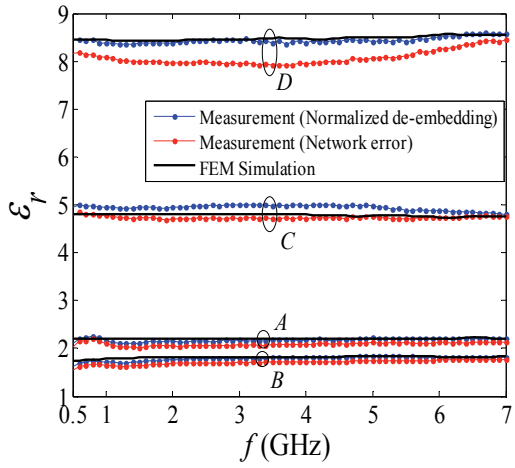

Fig. 8. Variations in relative dielectric constant, ε_r', with frequency, f, for four unknown samples.

calibration) using trial functions (11a) and (11b), respectively. Clearly, the different trial functions had a slight effect on the inversed values of ε_r'.

Fig. 10 shows the percentage of relative error, $|(\varepsilon_r - \varepsilon_{r\_meas})/\varepsilon_r| \times 100\%$, in the prediction of the dielectric constant from 0.5 to 7 GHz, which resulted from the uncertainty of the measured reflection coefficients (using network error calibration). The uncertainty of $|\mathrm{Re}(\Gamma - \Gamma_{BB'})/\mathrm{Re}(\Gamma)| \times 100\%$ did not seem to have an effect on

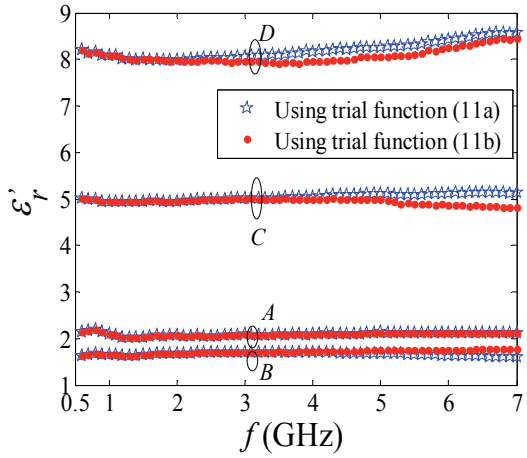

Fig. 9. Comparison of inversed relative dielectric constant, ε_r' using trial function (11a) and (11b).

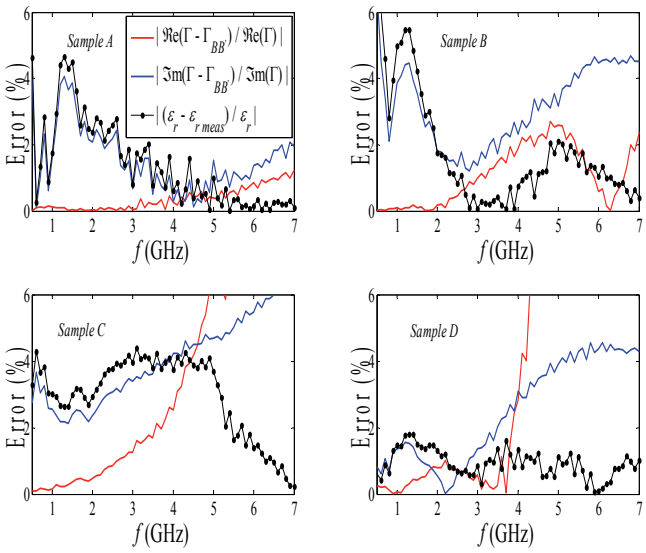

Fig. 10. Relationship of relative errors in the predictions of the dielectric constants, $|(\varepsilon_r - \varepsilon_{r\_meas})/\varepsilon_r|\times100\%$ and the relative errors in measured reflection coefficient, $\mathrm{Re}(\Gamma-\Gamma_{BB'})/\mathrm{Re}(\Gamma)|\times100\%$,$|\mathrm{Im}\,(\Gamma-\Gamma_{BB'})/\mathrm{Im}\,(\Gamma)|\times100\%$.

the errors in the predictions of the dielectric constants. In contrast, Fig. 6 shows that the influence of the uncertainty of $|\mathrm{Im}\,(\Gamma-\Gamma_{BB'})/\mathrm{Im}\,(\Gamma)|\times100\%$ was directly affected by the relative error of $|(\varepsilon_r-\varepsilon_{r\_meas})/\varepsilon_r|\times100\%$ below the operational frequency of 4 GHz. The uncertainties of $\mathrm{Re}(\Gamma-\Gamma_{BB'})/\mathrm{Re}(\Gamma)|\times100\%$ and $|\mathrm{Im}\,(\Gamma-\Gamma_{BB'})/\mathrm{Im}\,(\Gamma)|\times100\%$ were caused mainly by the quality of the measurements, which could have been affected by various factors, such as cable movements and small air gaps between the surfaces of the samples and the aperture of the probe. In addition, to the effects of the errors on the measurements of the reflection coefficient, the uncertainty in the predictions of the dielectric constants may have resulted from the fact that the actual coaxial probe was not perfect, even though it is represented as such in the FEM simulation; also, equation (1), which was based on the FEM simulation, was used as the dielectric inversion model.

6. Conclusions

Equation (1) was used successfully to predict the values of the dielectric constants of very thin, layered samples, with the thickness, h, of the sample being given. The technique was verified experimentally on four unknown, low-loss, dielectric samples for the frequency range of 0.5 to 7 GHz. It was very challenging to predict dielectric properties of the thin samples because they were so thin that they were very sensitive to any errors in the reflection measurements.

Acknowledgments

This study was supported by the Research University Grant (RUG) from Universiti Teknologi Malaysia under project number Q.J130000.2523.04H77 and the Ministry of Higher Education of Malaysia (MOHE).

References

[1] HASAR, U. C. Permittivity measurement of thin dielectric materials from reflection-only measurements using one-port vector network analyzers. *Progress in Electromagnetics Research*, 2009, vol. 95, p. 365–380.

[2] ALANEN, E., LAHTINEN, T., NUUTINEN, J. Variational formulation of open-ended coaxial line in contact with a layered biological medium. *IEEE Transactions on Biomedical Engineering,* 1998, vol. 45, no. 10, p. 1241–1248.

[3] NICOLSON, A. M., ROSS, G. F. Measurement of the intrinsic properties of materials by time-domain. *IEEE Transactions on Instrumentation Measurement*, 1970, vol. 19, no. 4, p. 377–382.

[4] WEIR, W. B. Automatic measurement of complex dielectric constant and permeability at microwave frequencies. *Proceedings of the IEEE,* 1974, vol. 62, no. 1, p. 33–36.

[5] BAKER-JARVIS, J., VANZURA, E. J., KISSICK W. A. Improved technique for determining complex permittivity with transmission/reflection method. *IEEE Transactions on Microwave Theory and Techniques,* 1990, vol. 38, no. 8, p. 1096–1103.

[6] CHALAPAT, K., SARVALA K., LI, J., PARAOANU, G. S. Wide reference-plane invariant method for measuring electromagnetic parameters of materials. *IEEE Transactions on Microwave Theory and Techniques,* 2009, vol. 57, no. 9, p. 2257–2267.

[7] IATROU, C. T., CAVENAGO, M. Field analysis of rectangular waveguide open junction. *IEEE Transactions on Microwave Theory and Techniques,* 1997, vol. 45, no. 2, p. 165–172.

[8] HYDE, M. W., HAVRILLA, M. J. Measurement of complex permittivity and permeability using two flanged rectangular waveguides. In *IEEE/MTT-S International Microwave Symposium*. Honolulu, (HI, USA), 3-8 June 2007.

[9] YOU, K. Y., ABBAS, Z., KHALID, K. Application of microwave moisture sensor for determination of oil palm fruit ripeness. *Measurement Science Review,* 2010, vol. 10, p. 7–14.

[10] WU, M. Z., YAO, X., ZHANG, L. Y. An improved coaxial probe technique for measuring microwave permittivity of thin dielectric materials. *Measurement Science and Technology*, 2000, vol. 11, p. 1617–1622.

[11] KRASZEWSKI, A., STUCHLY, M. A., STUCHLY, S. S. ANA calibration method for measurements of dielectric properties. *IEEE Transactions on Instrumentation Measurement,* 1983, vol. 32, no. 2, p. 385–386.

[12] GHANNOUCHI, F. M., MOHAMMADI A. *The Six-Port Technique with Microwave and Wireless Applications*. Norwood: Artech House, 2009, p. 113–117.

[13] BLACKHAM, D. V., POLLARD, R. D. An improved technique for permittivity measurements using a coaxial probe. *IEEE Transactions on Instrumentation Measurement,* 1997, vol. 46, no. 5, p. 1093–1099.

[14] JONSCHER, A. K. *Dielectric Relaxation in Solids*, London: Chelsea Dielectrics Press, 1983.

Appendix

	A_1		$A_2(f^{-1})$		$A_3(f^{-2})$		$A_4(f^{-3})$		$A_5(f^{-4})$		$A_6(f^{-5})$
η_0	1.137678976	α_0	$-7.174384419\times10^{-10}$	β_0	5.84953605×10^{-19}	γ_0	$-7.300482213\times10^{-29}$	σ_0	$-9.69945174\times10^{-39}$	χ_0	$1.387481423\times10^{-48}$
η_1	-2.496804026 (mm^{-1})	α_1	1.400425896×10^{-8} (mm^{-1})	β_1	$-1.321455272\times10^{-17}$ (mm^{-1})	γ_1	$3.013030643\times10^{-27}$ (mm^{-1})	σ_1	$-1.440657387\times10^{-37}$ (mm^{-1})	χ_1	$-6.506718621\times10^{-8}$ (mm^{-1})
η_2	16.217964374 (mm^{-2})	α_2	$-9.479166403\times10^{-8}$ (mm^{-2})	β_2	$9.558192050\times10^{-17}$ (mm^{-2})	γ_2	$-2.573560518\times10^{-26}$ (mm^{-2})	σ_2	$2.125220478\times10^{-36}$ (mm^{-2})	χ_2	$-2.841452872\times10^{-47}$ (mm^{-2})
η_3	-49.577642405 (mm^{-3})	α_3	2.977152619×10^{-7} (mm^{-3})	β_3	$-3.116385419\times10^{-16}$ (mm^{-3})	γ_3	$9.058064131\times10^{-26}$ (mm^{-3})	σ_3	$-8.78239945\times10^{-36}$ (mm^{-3})	χ_3	$2.228982801\times10^{-46}$ (mm^{-3})
η_4	72.890175760 (mm^{-4})	α_4	$-4.462811331\times10^{-7}$ (mm^{-4})	β_4	$4.785010214\times10^{-16}$ (mm^{-4})	γ_4	$-1.452655788\times10^{-25}$ (mm^{-4})	σ_4	$1.520783268\times10^{-35}$ (mm^{-4})	χ_4	$-4.637419948\times10^{-46}$ (mm^{-4})
η_5	-41.638803263 (mm^{-5})	α_5	2.587036734×10^{-7} (mm^{-5})	β_5	$-2.820454316\times10^{-16}$ (mm^{-5})	γ_5	$8.804307457\times10^{-26}$ (mm^{-5})	σ_5	$-9.63745234\times10^{-36}$ (mm^{-5})	χ_5	$3.208686456\times10^{-46}$ (mm^{-5})
η_6	$-8.476869639\times10^{-2}$	α_6	$3.968551071\times10^{-10}$	β_6	$-2.514545622\times10^{-19}$	γ_6	$-3.165556019\times10^{-29}$	σ_6	$1.961656879\times10^{-38}$	χ_6	$-1.614889391\times10^{-48}$
η_7	1.628592641 (mm^{-1})	α_7	$-8.468731665\times10^{-9}$ (mm^{-1})	β_7	$6.989649526\times10^{-18}$ (mm^{-1})	γ_7	$-8.542478603\times10^{-28}$ (mm^{-1})	σ_7	$-1.06174372\times10^{-37}$ (mm^{-1})	χ_7	$1.545499884\times10^{-47}$ (mm^{-1})
η_8	-10.944264964 (mm^{-2})	α_8	5.990178923×10^{-8} (mm^{-2})	β_8	$-5.459100314\times10^{-17}$ (mm^{-2})	γ_8	$1.076836252\times10^{-26}$ (mm^{-2})	σ_8	$-2.435513478\times10^{-37}$ (mm^{-2})	χ_8	$-4.754630520\times10^{-47}$ (mm^{-2})
η_9	34.250339804 (mm^{-3})	α_9	$-1.932872547\times10^{-7}$ (mm^{-3})	β_9	$1.853323360\times10^{-16}$ (mm^{-3})	γ_9	$-4.300991531\times10^{-26}$ (mm^{-3})	σ_9	$2.544011484\times10^{-36}$ (mm^{-3})	χ_9	$4.310243495\times10^{-47}$ (mm^{-3})
η_{10}	-51.243553259 (mm^{-4})	α_{10}	2.951774599×10^{-7} (mm^{-4})	β_{10}	$-2.918349732\times10^{-16}$ (mm^{-4})	γ_{10}	$7.348767626\times10^{-26}$ (mm^{-4})	σ_{10}	$-5.551898575\times10^{-36}$ (mm^{-4})	χ_{10}	$3.925554480\times10^{-47}$ (mm^{-4})
η_{11}	29.672536501 (mm^{-5})	α_{11}	$-1.734582527\times10^{-7}$ (mm^{-5})	β_{11}	$1.750175001\times10^{-16}$ (mm^{-5})	γ_{11}	$-4.627140958\times10^{-26}$ (mm^{-5})	σ_{11}	$3.922264336\times10^{-36}$ (mm^{-5})	χ_{11}	$-6.47483795\times10^{-47}$ (mm^{-5})
η_{12}	1.198533901×10^{-2}	α_{12}	$-3.913268461\times10^{-11}$	β_{12}	$-2.429981611\times10^{-20}$	γ_{12}	$3.217569122\times10^{-29}$	σ_{12}	$-7.28932584\times10^{-39}$	χ_{12}	$4.765811711\times10^{-49}$
η_{13}	$-2.617748871\times10^{-1}$ (mm^{-1})	α_{13}	1.127463728×10^{-9} (mm^{-1})	β_{13}	$-3.18246809\times10^{-19}$ (mm^{-1})	γ_{13}	$-2.458348130\times10^{-28}$ (mm^{-1})	σ_{13}	$7.999395281\times10^{-38}$ (mm^{-1})	χ_{13}	$-5.944504765\times10^{-48}$ (mm^{-1})
η_{14}	1.869925598 (mm^{-2})	α_{14}	$-8.885874782\times10^{-9}$ (mm^{-2})	β_{14}	$4.739124892\times10^{-18}$ (mm^{-2})	γ_{14}	$3.655001739\times10^{-28}$ (mm^{-2})	σ_{14}	$-3.216837424\times10^{-37}$ (mm^{-2})	χ_{14}	$2.809325398\times10^{-47}$ (mm^{-2})
η_{15}	-6.064922598 (mm^{-3})	α_{15}	3.030102394×10^{-8} (mm^{-3})	β_{15}	$-1.959032525\times10^{-17}$ (mm^{-3})	γ_{15}	$1.225128749\times10^{-27}$ (mm^{-3})	σ_{15}	$6.035792922\times10^{-37}$ (mm^{-3})	χ_{15}	$-6.552445075\times10^{-47}$ (mm^{-3})
η_{16}	9.29057809 (mm^{-4})	α_{16}	$-4.784895412\times10^{-8}$ (mm^{-4})	β_{16}	3.39568064×10^{-17} (mm^{-4})	γ_{16}	$-4.140019751\times10^{-27}$ (mm^{-4})	σ_{16}	$-5.086583342\times10^{-37}$ (mm^{-4})	χ_{16}	$7.602488997\times10^{-47}$ (mm^{-4})
η_{17}	-5.470450232 (mm^{-5})	α_{17}	2.875392541×10^{-8} (mm^{-5})	β_{17}	$-2.154742793\times10^{-17}$ (mm^{-5})	γ_{17}	$3.328573492\times10^{-27}$ (mm^{-5})	σ_{17}	$1.351965847\times10^{-37}$ (mm^{-5})	χ_{17}	$-3.511505529\times10^{-47}$ (mm^{-5})
η_{18}	$-3.553651117\times10^{-4}$	α_{18}	$-6.960658498\times10^{-13}$	β_{18}	$5.132942667\times10^{-21}$	γ_{18}	$-3.228471732\times10^{-30}$	σ_{18}	6.1987191×10^{-40}	χ_{18}	$-3.766348885\times10^{-50}$
η_{19}	1.127323101×10^{-2} (mm^{-1})	α_{19}	$-2.570618736\times10^{-11}$ (mm^{-1})	β_{19}	$-3.812202685\times10^{-20}$ (mm^{-1})	γ_{19}	$3.694556223\times10^{-29}$ (mm^{-1})	σ_{19}	$-8.133263075\times10^{-39}$ (mm^{-1})	χ_{19}	$5.306760013\times10^{-49}$ (mm^{-1})
η_{20}	$-9.146445647\times10^{-2}$ (mm^{-2})	α_{20}	$3.099260942\times10^{-10}$ (mm^{-2})	β_{20}	$4.502034254\times10^{-20}$ (mm^{-2})	γ_{20}	$-1.567581658\times10^{-28}$ (mm^{-2})	σ_{20}	$4.033848910\times10^{-38}$ (mm^{-2})	χ_{20}	$-2.815315443\times10^{-48}$ (mm^{-2})
η_{21}	3.159763324×10^{-1} (mm^{-3})	α_{21}	$-1.227925332\times10^{-9}$ (mm^{-3})	β_{21}	$2.507133070\times10^{-19}$ (mm^{-3})	γ_{21}	$3.186318282\times10^{-28}$ (mm^{-3})	σ_{21}	$-9.890012523\times10^{-38}$ (mm^{-3})	χ_{21}	$7.358225420\times10^{-48}$ (mm^{-3})
η_{22}	$-5.024342061\times10^{-1}$ (mm^{-4})	α_{22}	2.093334242×10^{-9} (mm^{-4})	β_{22}	$-7.582190607\times10^{-19}$ (mm^{-4})	γ_{22}	$-3.079346108\times10^{-28}$ (mm^{-4})	σ_{22}	$1.209501746\times10^{-37}$ (mm^{-4})	χ_{22}	$-9.565310006\times10^{-48}$ (mm^{-4})
η_{23}	3.031657214×10^{-1} (mm^{-5})	α_{23}	$-1.317250312\times10^{-9}$ (mm^{-5})	β_{23}	$5.941497062\times10^{-19}$ (mm^{-5})	γ_{23}	$1.099717314\times10^{-28}$ (mm^{-5})	σ_{23}	$-5.906593807\times10^{-38}$ (mm^{-5})	χ_{23}	$4.951049919\times10^{-48}$ (mm^{-5})
η_{24}	2.060325131×10^{-7}	α_{24}	6.13810462×10^{-14}	β_{24}	$-1.538769797\times10^{-22}$	γ_{24}	$8.197907995\times10^{-32}$	σ_{24}	$-1.478240481\times10^{-41}$	χ_{24}	$8.689655504\times10^{-52}$
η_{25}	$-1.263437901\times10^{-4}$ (mm^{-1})	α_{25}	$-2.290879414\times10^{-13}$ (mm^{-1})	β_{25}	$1.650856406\times10^{-21}$ (mm^{-1})	γ_{25}	$-1.068403377\times10^{-30}$ (mm^{-1})	σ_{25}	$2.109967011\times10^{-40}$ (mm^{-1})	χ_{25}	$-1.30935851\times10^{-50}$ (mm^{-1})
η_{26}	1.295088408×10^{-3} (mm^{-2})	α_{26}	$-1.90266234\times10^{-12}$ (mm^{-2})	β_{26}	$-6.353196305\times10^{-21}$ (mm^{-2})	γ_{26}	$5.258504738\times10^{-30}$ (mm^{-2})	σ_{26}	$-1.130328088\times10^{-39}$ (mm^{-2})	χ_{26}	$7.342262493\times10^{-50}$ (mm^{-2})
η_{27}	$-4.906190645\times10^{-3}$ (mm^{-3})	α_{27}	$1.249950704\times10^{-11}$ (mm^{-3})	β_{27}	$1.0938935570\times10^{-20}$ (mm^{-3})	γ_{27}	$-1.277751969\times10^{-29}$ (mm^{-3})	σ_{27}	$2.977052018\times10^{-39}$ (mm^{-3})	χ_{27}	$-2.009974235\times10^{-49}$ (mm^{-3})
η_{28}	8.194138917×10^{-3} (mm^{-4})	α_{28}	$-2.521870626\times10^{-11}$ (mm^{-4})	β_{28}	$-7.548539233\times10^{-21}$ (mm^{-4})	γ_{28}	$1.5470641676\times10^{-29}$ (mm^{-4})	σ_{28}	$-3.89444317\times10^{-39}$ (mm^{-4})	χ_{28}	$2.717871721\times10^{-49}$ (mm^{-4})
η_{29}	$-5.096381229\times10^{-3}$ (mm^{-5})	α_{29}	$1.727670528\times10^{-11}$ (mm^{-5})	β_{29}	$7.878796629\times10^{-22}$ (mm^{-5})	γ_{29}	$-7.4740476512\times10^{-30}$ (mm^{-5})	σ_{29}	$2.026440077\times10^{-39}$ (mm^{-5})	χ_{29}	$-1.455195765\times10^{-49}$ (mm^{-5})

Tab. 1. Coefficients for Equation (2a).

B_1		$B_2\ (f^{-1})$		$B_3\ (f^{-2})$		$B_4\ (f^{-3})$		$B_5\ (f^{-4})$		$B_6\ (f^{-5})$	
ζ_0	8.413306712×10^{-2}	ξ_0	$-8.351656065\times10^{-10}$	Ψ_0	$1.192802807\times10^{-18}$	τ_0	$-5.432131914\times10^{-28}$	ν_0	8.66728061×10^{-38}	ρ_0	-4.5789707×10^{-48}
ζ_1	$-8.652445733\times10^{-1}$ (mm^{-1})	ξ_1	1.025827244×10^{-8} (mm^{-1})	Ψ_1	$-1.69226950\times10^{-17}$ (mm^{-1})	τ_1	$8.318256698\times10^{-27}$ (mm^{-1})	ν_1	$-1.404482894\times10^{-36}$ (mm^{-1})	ρ_1	$7.732592743\times10^{-47}$ (mm^{-1})
ζ_2	2.916522763 (mm^{-2})	ξ_2	$-4.900627747\times10^{-8}$ (mm^{-2})	Ψ_2	$9.130959406\times10^{-17}$ (mm^{-2})	τ_2	$-4.773663498\times10^{-26}$ (mm^{-2})	ν_2	$8.378015908\times10^{-36}$ (mm^{-2})	ρ_2	$-4.736883505\times10^{-46}$ (mm^{-2})
ζ_3	-3.137172588 (mm^{-3})	ξ_3	1.14293539×10^{-7} (mm^{-3})	Ψ_3	$-2.410581539\times10^{-16}$ (mm^{-3})	τ_3	$1.329466089\times10^{-25}$ (mm^{-3})	ν_3	$-2.401270467\times10^{-35}$ (mm^{-3})	ρ_3	$1.382522843\times10^{-45}$ (mm^{-3})
ζ_4	-1.709149086 (mm^{-4})	ξ_4	$-1.305052822\times10^{-7}$ (mm^{-4})	Ψ_4	$3.142359429\times10^{-16}$ (mm^{-4})	τ_4	$-1.817727007\times10^{-25}$ (mm^{-4})	ν_4	$3.358333112\times10^{-35}$ (mm^{-4})	ρ_4	$-1.959357434\times10^{-45}$ (mm^{-4})
ζ_5	3.767862684 (mm^{-5})	ξ_5	5.834828784×10^{-8} (mm^{-5})	Ψ_5	$-1.622500347\times10^{-16}$ (mm^{-5})	τ_5	$9.797655711\times10^{-26}$ (mm^{-5})	ν_5	$-1.843897715\times10^{-35}$ (mm^{-5})	ρ_5	$1.086773425\times10^{-45}$ (mm^{-5})
ζ_6	$-7.966357239\times10^{-2}$	ξ_6	$4.528687099\times10^{-10}$	Ψ_6	$-9.330114082\times10^{-19}$	τ_6	$3.936384739\times10^{-28}$	ν_6	$-5.90573454\times10^{-38}$	ρ_6	$2.990152241\times10^{-48}$
ζ_7	9.929630347×10^{-1} (mm^{-1})	ξ_7	$-7.327337322\times10^{-9}$ (mm^{-1})	Ψ_7	$1.403212075\times10^{-17}$ (mm^{-1})	τ_7	$-6.342412617\times10^{-27}$ (mm^{-1})	ν_7	1.0084571×10^{-36} (mm^{-1})	ρ_7	$-5.341044259\times10^{-47}$ (mm^{-1})
ζ_8	-4.650435459 (mm^{-2})	ξ_8	3.988950674×10^{-8} (mm^{-2})	Ψ_8	$-7.99534251\times10^{-17}$ (mm^{-2})	τ_8	$3.789418823\times10^{-26}$ (mm^{-2})	ν_8	$-6.244073032\times10^{-36}$ (mm^{-2})	ρ_8	$3.396954075\times10^{-46}$ (mm^{-2})
ζ_9	10.4837820524 (mm^{-3})	ξ_9	-1.04470778×10^{-7} (mm^{-3})	Ψ_9	$2.222608542\times10^{-16}$ (mm^{-3})	τ_9	$-1.092074366\times10^{-25}$ (mm^{-3})	ν_9	$1.843264761\times10^{-35}$ (mm^{-3})	ρ_9	$-1.020154984\times10^{-45}$ (mm^{-3})
ζ_{10}	-11.425418839 (mm^{-4})	ξ_{10}	1.344820448×10^{-7} (mm^{-4})	Ψ_{10}	$-3.041019233\times10^{-16}$ (mm^{-4})	τ_{10}	$1.537810115\times10^{-25}$ (mm^{-4})	ν_{10}	$-2.641265206\times10^{-35}$ (mm^{-4})	ρ_{10}	$1.479243757\times10^{-45}$ (mm^{-4})
ζ_{11}	4.796161336 (mm^{-5})	ξ_{11}	$-6.848950237\times10^{-8}$ (mm^{-5})	Ψ_{11}	1.64223392×10^{-16} (mm^{-5})	τ_{11}	$-8.502625685\times10^{-26}$ (mm^{-5})	ν_{11}	$1.479866386\times10^{-35}$ (mm^{-5})	ρ_{11}	$-8.359964813\times10^{-46}$ (mm^{-5})
ζ_{12}	2.071774853×10^{-2}	ξ_{12}	$-1.501746867\times10^{-10}$	Ψ_{12}	$1.982377175\times10^{-19}$	τ_{12}	$-7.152226424\times10^{-29}$	ν_{12}	$9.817208094\times10^{-39}$	ρ_{12}	$-4.654791231\times10^{-49}$
ζ_{13}	$-2.916624851\times10^{-1}$ (mm^{-1})	ξ_{13}	2.282953944×10^{-9} (mm^{-1})	Ψ_{13}	$-3.181903759\times10^{-18}$ (mm^{-1})	τ_{13}	$1.246194525\times10^{-27}$ (mm^{-1})	ν_{13}	$-1.831667845\times10^{-37}$ (mm^{-1})	ρ_{13}	$9.201418052\times10^{-48}$ (mm^{-1})
ζ_{14}	1.564210842 (mm^{-2})	ξ_{14}	$-1.307574416\times10^{-8}$ (mm^{-2})	Ψ_{14}	$1.903835959\times10^{-17}$ (mm^{-2})	τ_{14}	$-7.806515018\times10^{-27}$ (mm^{-2})	ν_{14}	$1.191523564\times10^{-36}$ (mm^{-2})	ρ_{14}	$-6.173352562\times10^{-47}$ (mm^{-2})
ζ_{15}	-4.113754388 (mm^{-3})	ξ_{15}	3.653679384×10^{-8} (mm^{-3})	Ψ_{15}	$-5.505210224\times10^{-17}$ (mm^{-3})	τ_{15}	$2.325492555\times10^{-26}$ (mm^{-3})	ν_{15}	$-3.632831622\times10^{-36}$ (mm^{-3})	ρ_{15}	$1.917091301\times10^{-46}$ (mm^{-3})
ζ_{16}	5.350859158 (mm^{-4})	ξ_{16}	$-5.025935902\times10^{-8}$ (mm^{-4})	Ψ_{16}	$7.782482573\times10^{-17}$ (mm^{-4})	τ_{16}	$-3.357331783\times10^{-26}$ (mm^{-4})	ν_{16}	$5.327505449\times10^{-36}$ (mm^{-4})	ρ_{16}	$-2.845358428\times10^{-46}$ (mm^{-4})
ζ_{17}	-2.759781872 (mm^{-5})	ξ_{17}	2.728788081×10^{-8} (mm^{-5})	Ψ_{17}	$-4.319561238\times10^{-17}$ (mm^{-5})	τ_{17}	$1.892904205\times10^{-26}$ (mm^{-5})	ν_{17}	$-3.037596782\times10^{-36}$ (mm^{-5})	ρ_{17}	$1.635996285\times10^{-46}$ (mm^{-5})
ζ_{18}	$-1.582542111\times10^{-3}$	ξ_{18}	1.04005705×10^{-11}	Ψ_{18}	$-1.182903396\times10^{-20}$	τ_{18}	$3.901588182\times10^{-30}$	ν_{18}	$-4.95339455\times10^{-40}$	ρ_{18}	$2.168196026\times10^{-50}$
ζ_{19}	2.422804846×10^{-2} (mm^{-1})	ξ_{19}	$-1.699463899\times10^{-10}$ (mm^{-1})	Ψ_{19}	$2.065296692\times10^{-19}$ (mm^{-1})	τ_{19}	$-7.472163928\times10^{-29}$ (mm^{-1})	ν_{19}	$1.036081659\times10^{-38}$ (mm^{-1})	ρ_{19}	$-4.947167007\times10^{-49}$ (mm^{-1})
ζ_{20}	$-1.391488565\times10^{-1}$ (mm^{-2})	ξ_{20}	1.023706267×10^{-9} (mm^{-2})	Ψ_{20}	$-1.296867855\times10^{-18}$ (mm^{-2})	τ_{20}	$4.924018639\times10^{-28}$ (mm^{-2})	ν_{20}	$-7.13583412\times10^{-38}$ (mm^{-2})	ρ_{20}	$3.546946404\times10^{-48}$ (mm^{-2})
ζ_{21}	3.883617049×10^{-1} (mm^{-3})	ξ_{21}	$-2.970734046\times10^{-9}$ (mm^{-3})	Ψ_{21}	$3.870974101\times10^{-18}$ (mm^{-3})	τ_{21}	$-1.513277786\times10^{-27}$ (mm^{-3})	ν_{21}	2.24975577×10^{-37} (mm^{-3})	ρ_{21}	$-1.143402562\times10^{-47}$ (mm^{-3})
ζ_{22}	$-5.325561999\times10^{-1}$ (mm^{-4})	ξ_{22}	4.209529618×10^{-9} (mm^{-4})	Ψ_{22}	$-5.597615443\times10^{-18}$ (mm^{-4})	τ_{22}	2.23144326×10^{-27} (mm^{-4})	ν_{22}	$-3.372527047\times10^{-37}$ (mm^{-4})	ρ_{22}	$1.738004962\times10^{-47}$ (mm^{-4})
ζ_{23}	2.879846965×10^{-1} (mm^{-5})	ξ_{23}	-2.34068299×10^{-9} (mm^{-5})	Ψ_{23}	$3.160150824\times10^{-18}$ (mm^{-5})	τ_{23}	$-1.277462455\times10^{-27}$ (mm^{-5})	ν_{23}	$1.952870457\times10^{-37}$ (mm^{-5})	ρ_{23}	$-1.015890931\times10^{-47}$ (mm^{-5})
ζ_{24}	3.478055264×10^{-5}	ξ_{24}	$-2.127593249\times10^{-13}$	Ψ_{24}	$2.224762248\times10^{-22}$	τ_{24}	$-6.818567797\times10^{-32}$	ν_{24}	$7.957270484\times10^{-42}$	ρ_{24}	$-3.124299375\times10^{-52}$
ζ_{25}	$-5.631715056\times10^{-4}$ (mm^{-1})	ξ_{25}	$3.672929672\times10^{-12}$ (mm^{-1})	Ψ_{25}	$-4.139360454\times10^{-21}$ (mm^{-1})	τ_{25}	$1.416071576\times10^{-30}$ (mm^{-1})	ν_{25}	$-1.864360933\times10^{-40}$ (mm^{-1})	ρ_{25}	$8.433382773\times10^{-51}$ (mm^{-1})
ζ_{26}	3.368464237×10^{-3} (mm^{-2})	ξ_{26}	$-2.292358447\times10^{-11}$ (mm^{-2})	Ψ_{26}	$2.696313534\times10^{-20}$ (mm^{-2})	τ_{26}	$-9.734779012\times10^{-30}$ (mm^{-2})	ν_{26}	$1.353148992\times10^{-39}$ (mm^{-2})	ρ_{26}	$-6.466199472\times10^{-50}$ (mm^{-2})
ζ_{27}	$-9.697354478\times10^{-3}$ (mm^{-3})	ξ_{27}	$6.816712277\times10^{-11}$ (mm^{-3})	Ψ_{27}	$-8.237396432\times10^{-20}$ (mm^{-3})	τ_{27}	$3.068039944\times10^{-29}$ (mm^{-3})	ν_{27}	$-4.393315231\times10^{-39}$ (mm^{-3})	ρ_{27}	$2.159420882\times10^{-49}$ (mm^{-3})
ζ_{28}	1.363042892×10^{-2} (mm^{-4})	ξ_{28}	$-9.832944745\times10^{-11}$ (mm^{-4})	Ψ_{28}	$1.210350253\times10^{-19}$ (mm^{-4})	τ_{28}	$-4.599654961\times10^{-29}$ (mm^{-4})	ν_{28}	$6.709669741\times10^{-39}$ (mm^{-4})	ρ_{28}	$-3.354157967\times10^{-49}$ (mm^{-4})
ζ_{29}	$-7.521005628\times10^{-3}$ (mm^{-5})	ξ_{29}	5.54197071×10^{-11} (mm^{-5})	Ψ_{29}	$-6.912751653\times10^{-20}$ (mm^{-5})	τ_{29}	$2.664076191\times10^{-29}$ (mm^{-5})	ν_{29}	$-3.93516411\times10^{-39}$ (mm^{-5})	ρ_{29}	$1.989183898\times10^{-49}$ (mm^{-5})

Tab. 2. Coefficients for Equation (2b).